Komatiite Flooding of a Rifted Archean Rhyolitic Arc Complex: Geochemical Signature and Tectonic Significance of the Stoughton-Roquemaure Group, Abitibi Greenstone Belt, Canada[1]

J. Dostal and W. U. Mueller[2]

Department of Geology, Saint Mary's University, Halifax, Nova Scotia, Canada B3H 3C3

ABSTRACT

The 0.2–2 km thick, Archean Stoughton-Roquemaure Group (SRG) in the Northern Volcanic Zone of the Abitibi greenstone belt (Quebec, Canada) is composed of tholeiitic basalt, komatiitic basalt and komatiite. The mafic and ultramafic rocks are pillowed, brecciated, and massive columnar-jointed flows. The SRG conformably overlies the 2730 Ma Hunter Mine Group, a volcanic complex dominated by calc-alkaline felsic rocks. The tholeiitic basalts of the SRG resemble MORB. The komatiitic basalts and komatiites have positive ϵ_{Nd} values, overlapping those of the tholeiitic basalts. Komatiitic basalts, with low Al_2O_3/TiO_2 ratios (~10) and fractionated heavy REE patterns, are similar to Al-depleted komatiites. In contrast, the komatiites have high Al_2O_3/TiO_2 (~20), unfractionated heavy REE patterns and resemble Al-undepleted Munro-type komatiites. The Al-depleted komatiitic basalts occur at the base of the SRG, whereas the Al-undepleted komatiites are prevalent higher up in the stratigraphy. The association of calc-alkaline rhyolites with rifted arc-related basalts passing upward into MORB-like basalts, which in turn are capped by komatiitic rocks, reflects an evolution in magma genesis from crustal melting (rhyolites) and arc rifting to melting of a mantle plume. The preferred petrogenetic model for the SRG involves a rising mantle plume below an arc. The Al-depleted komatiitic basalts were generated by mantle melting with garnet in the residue at the periphery of the plume whereas the Al-undepleted komatiites were formed by a higher degree of melting in the plume axis. The MORB-like basalts were produced from the cooler plume head at a shallower depth.

Introduction

Komatiites and komatiitic basalts have attracted much attention, largely because they indicate the composition, structure, and physical conditions of the Archean mantle (e.g., Arndt 1994). Numerous studies of komatiites dealing with their stratigraphic position (Anhaeusser 1971), geochemistry (Arndt and Nisbet 1982), and inferred genesis (Campbell et al. 1989; Arndt 1994) have been published, but the geodynamic environment of komatiites remains enigmatic. Two distinct tectonic settings have been recognized: (1) rifting of a stable continental landmass, and (2) rifting of oceanic lithosphere.

The komatiites of the Bend (Bickle and Nisbet 1993) and Reliance (Bickle et al. 1994) Formations of the 2.9 Ga Mtshingwe and 2.7 Ga Ngezi Groups, respectively, of the Belingwe greenstone belt (Zimbabwe Craton) were inferred to have formed in a shallow water, continental, rift-type setting. Stable platformal conditions were suggested for komatiites associated with quartz arenites in >2.8 Ga greenstone belts of the Superior Province of the Canadian Shield (Thurston and Chivers 1990).

Alternatively, komatiites are an integral component of the Archean ocean floor, as suggested for the Barberton (de Wit et al. 1987) and Abitibi greenstone belts (Dupre et al. 1984). Recently, Storey et al. (1991) proposed that komatiites could be parts of oceanic plateaus, whereas Takahashi (1990) suggested that komatiites formed at mid-ocean ridges. In contrast, komatiitic basalts and komatiites of the Stoughton-Roquemaure Group (SRG) in the Archean Abitibi greenstone belt (Quebec, Canada) are interpreted in this study to represent a third tectonic setting: komatiite flooding of a rifted subaqueous volcanic arc complex.

The purpose of this paper is (1) to characterize geochemically the komatiitic basalts and komati-

[1] Manuscript received July 11, 1996; accepted April 1, 1997.

[2] Sciences de la Terre, Université du Québec à Chicoutimi, Quebec, Canada G7H 2B1.

[The Journal of Geology, 1997, volume 105, p. 545–563] 0022-1376/97/10504-0003$01.00

ites of the SRG, (2) to describe the physical volcanology of the komatiitic basalts and komatiites, (3) to discuss the evolution of these rocks, and (4) to propose an appropriate geodynamic model for this part of the Abitibi greenstone belt. Special emphasis is placed on establishing the geochemical signature and the geodynamic setting of basaltic and komatiitic rocks from a rhyolite/basalt/komatiite succession in this greenstone belt.

Regional Geology

The Abitibi greenstone belt, the largest coherent Archean supracrustal sequence in the world, has been divided into Northern Volcanic (NVZ) and Southern Volcanic zones (SVZ; Chown et al. 1992); the study area is located at the southernmost part of the NVZ (figure 1). The 2730–2705 Ma NVZ is considered to be an intact arc-backarc segment separated from the volcanic terranes of the 2705–2695 Ma SVZ by the crustal-scale Destor-Porcupine-Manneville fault (figures 1 and 2; Mueller et al. 1996). The NVZ consists of two 1–5 km thick mafic-felsic volcanic cycles (Chown et al. 1992). Volcanic cycle 1 represents an extensive subaqueous basalt plain with local mafic-felsic or felsic edifices interstratified with or overlain by intra-arc, volcaniclastic turbidites (Mueller et al. 1996). These volcanic edifices are inferred to be ancient submarine composite volcanoes. The felsic-dominated volcanic centers yield U-Pb zircon ages ranging from 2730 to 2720 Ma (Mortensen 1993*a,* 1993*b*). Volcanic cycle 2 (2720–2705 Ma; Mortensen 1993*a,* 1993*b*), preserved in the northern and southern extremities of the NVZ (figure 1), displays the evolved stages of arc development with the emergence and unroofing of the arc (Mueller et al. 1989), as indicated by coarse clastic deposits (Mueller and Donaldson 1992*a*). The 4–5 km thick Hunter Mine Group (HMG), a 2730 Ma volcanic complex which can be traced along a strike for 50 km, is part of volcanic cycle 1. The SRG volcanic rocks may represent the beginning of volcanic cycle 2 or may be still part of volcanic cycle 1. The basal to medial parts of the HMG are composed of 5–50 m thick massive to brecciated rhyolitic lava flows and lobes (Dostal and Mueller 1996) and an extensive, 1.5 km wide, felsic-dominated, dike swarm that can be traced for 2.5 km up-section (Mueller and Donaldson 1992b). Mafic dikes of SRG- affinity are part of this swarm (e.g., sample S-32, table 2 in Dostal and Mueller 1996), suggesting a prolonged dike emplacement history that includes feeding of the SRG volcanic flows.

The upper 500–1000 m thick transition zone of the HMG, directly above the dike system (figure 2), is a highly variable association of pyroclastic and volcaniclastic sedimentary rocks, iron-formation, mafic to intermediate dikes, and sills (table 1, samples J-26 and J-28) and mafic (table 1, samples WP-94-05, WP-94-27) and felsic lava flows (table 1, sample WP-94-10). The mafic flow component increases toward the SRG. Complex on-lapping (e.g., Eakins 1972) and interstratification between groups is common to volcanic terranes (Mueller et al. 1989).

The mafic-ultramafic SRG (table 1, series Roq-95) is only 200 m thick directly above the 4–5 km thick central part of the HMG, whereas immediately to the west, its thickness increases to 2 km. The HMG thins accordingly. The Lyndhurst fault truncates both the HMG and SRG along strike (figure 2), which explains the limited thickness of the SRG above the central part of the HMG. Goutier (1993) identified two lithological units. The alternating 50–400 m thick komatiitic and 100–1000 m thick basaltic units can be traced for several kilometers (figure 2). The ultramafic flows are possibly the lateral on-strike equivalents of the well-documented komatiite flows in Munro Township to the west (figure 1; Pyke et al. 1973; Arndt et al. 1977). U-Pb zircon age determinations of 2713 Ma and 2714 Ma from felsic volcanic rocks inferred to be associated with the Munro Township ultramafic assemblage (Corfu et al. 1989) constrain the minimum age of the SRG.

The SRG and transition zone rocks of the HMG in the study area were affected mainly by subgreenschist facies metamorphism, as characterized by the assemblage of prehnite-chlorite-epidote. The volcano-sedimentary rocks of the HMG and SRG are steeply dipping sequences (70–90°) with locally overturned strata that young to the south in the study area. Both formations trace a large anticline that closes to the west (Eakins 1972; figure 2). The steeply dipping strata expose a cross-section of the felsic-dominated submarine volcanic complex showing a N-trending central dike swarm represented by the HMG and a subaqueous, mafic-ultramafic, oceanic plain represented by the SRG.

Physical Volcanology of Mafic-Ultramafic Flows

The flow morphology of mafic-ultramafic lava flows depends on composition, temperature, viscosity, and extrusion rate (e.g., Donaldson 1982; Arndt 1994). The lava flow description helps to explain geochemical variations in different flow forms, facilitate interpretation of the volcanic flow

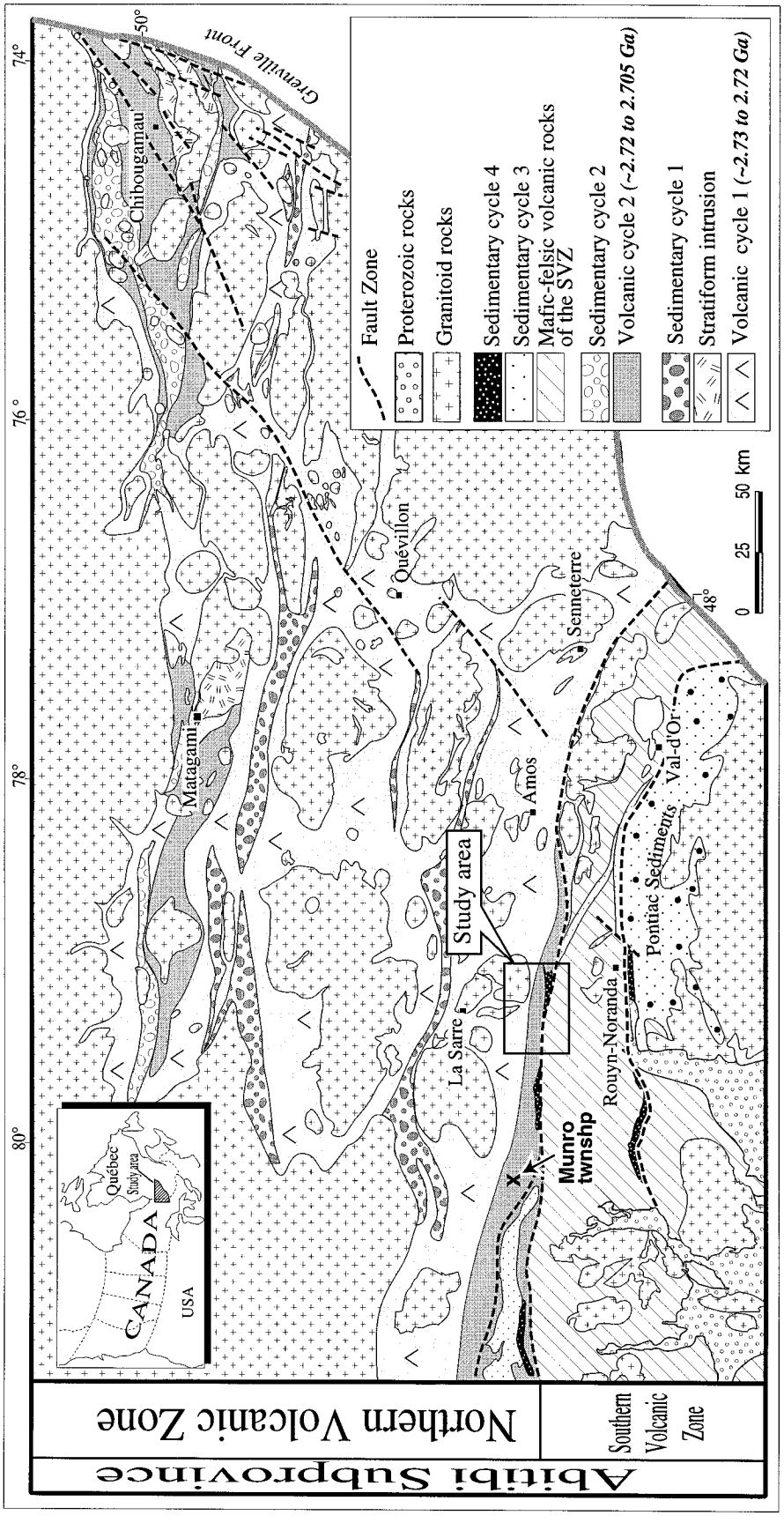

Figure 1. General geology of the Abitibi greenstone belt including Northern (NVZ) and Southern Volcanic zones (SVZ). Outlined study area (figure 2) is located in the southern extremity of the NVZ. The supracrustal sequence is divided into different volcanic and sedimentary cycles. Munro Township komatiites are laterally on strike with the Stoughton-Roquemaure Group ultramafic flows.

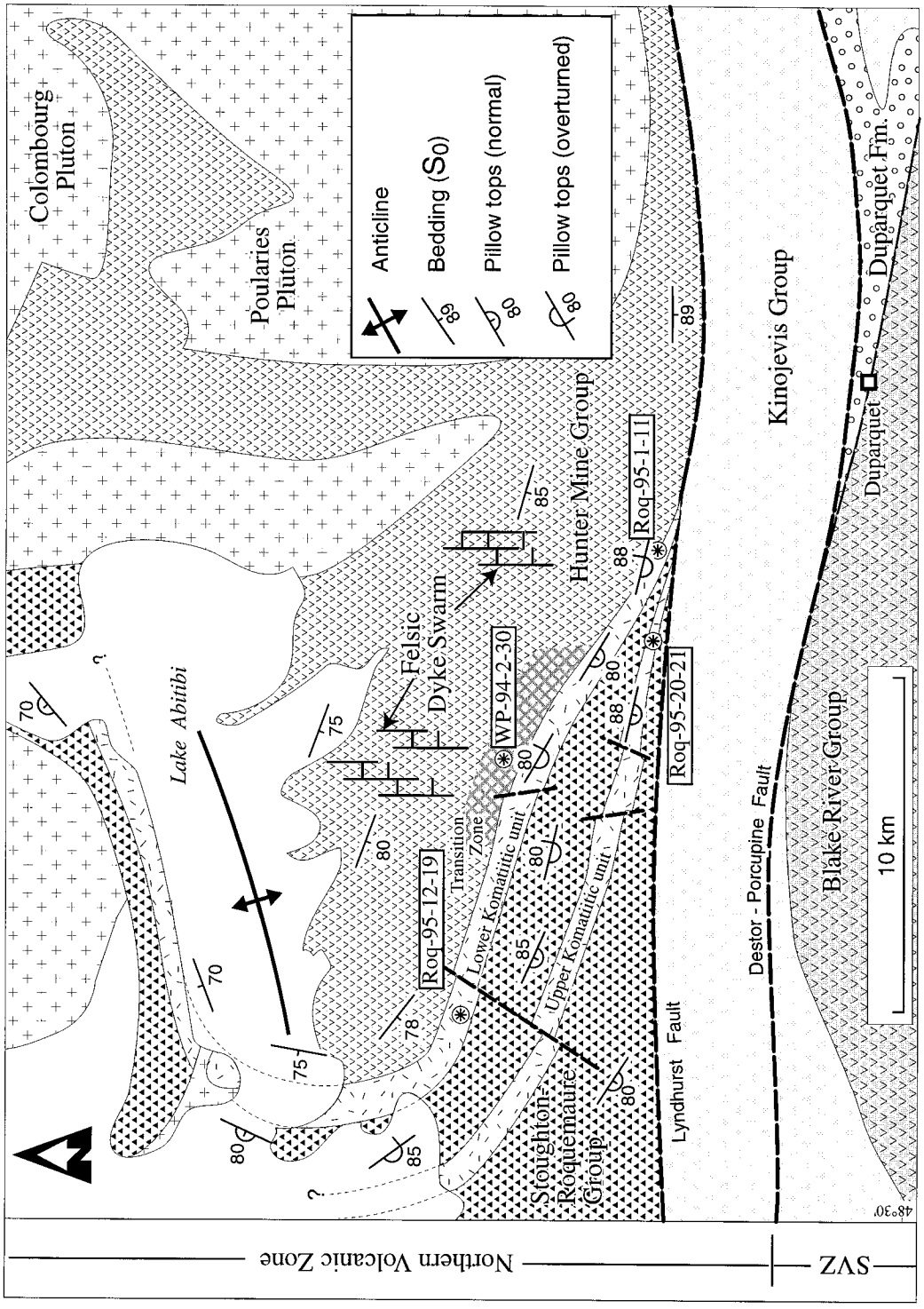

Figure 2. Geological map of the study area at the southern extremity of the Northern Volcanic Zone (NVZ). The volcanic complex of the Hunter Mine Group (HMG) and its transition zone is overlain by the Stoughton-Roquemaure Group (SRG). The two SRG komatiite units can be traced to the north. Sampled areas are indicated by stars. The map modified after Eakins (1972), Goutier (1993), and our field work.

Table 1. Major and Trace Element Composition of Representative Rocks of Stoughton-Roquemaure and Hunter Mine Groups

	SRG							Transition Zone						HMG		
	Komatiic Basalt					Komatiite		MORB like Basalt				High Mg Basalt		RAB	AD	Rhyolite
Sample (%, ppm)	Roq-95-7	Roq-95-10	Roq-95-11	Roq-95-12	Roq-95-17	Roq-95-15	Roq-95-20	WP-94-06	WP-94-12	WP-94-13	WP-94-26	WP-94-5	WP-94-27	J-26	J-28	WP-94-10
SiO_2	48.24	47.13	48.22	45.56	45.49	43.35	41.51	47.45	48.35	46.24	47.18	47.27	49.88	52.41	57.07	74.51
TiO_2	.80	.83	.86	.70	.83	.48	.50	.92	.88	.88	.90	.66	.62	1.34	.86	.18
Al_2O_3	8.76	9.26	9.30	7.86	7.87	9.47	10.05	15.06	14.62	14.79	15.09	14.87	13.73	15.44	15.94	11.41
FeO*	11.24	11.42	11.41	11.62	12.57	10.54	10.99	12.48	11.50	11.65	11.37	10.55	10.96	10.27	7.38	4.59
MnO	.18	.19	.17	.18	.22	.17	.18	.23	.21	.20	.20	.20	.19	.16	.12	.09
MgO	15.73	15.71	14.61	18.12	17.92	21.13	21.37	8.21	7.31	7.36	6.92	9.41	9.28	6.49	6.12	1.73
CaO	8.61	9.34	9.13	9.73	8.38	7.59	7.98	8.73	10.51	12.67	11.68	8.94	8.57	5.78	6.63	.25
Na_2O	1.44	1.12	1.84	.36	.56	.16	.02	3.29	2.64	1.37	2.47	1.96	3.54	3.59	1.96	4.94
K_2O	.01	.02	.05	.01	.03	.01		.03	.07		.03	.40		.14	.90	.04
P_2O_5	.06	.05	.06	.05	.05	.04	.04	.06	.06	.06	.05	.04	.04	.25	.20	.03
LOI	3.90	4.00	3.80	4.60	5.40	6.20	6.30	3.00	3.50	3.70	3.60	4.70	3.40	3.30	2.20	1.40
Σ	98.97	99.08	99.46	98.79	99.32	99.14	98.94	99.46	99.65	98.92	99.49	99.00	100.21	99.17	99.38	99.16
Mg#	71.4	71.0	69.5	73.5	71.7	78.1	77.6	54.0	53.1	52.9	52.0	61.4	60.1	53.0	59.6	40.2
Cr	1531	1687	1506	1876	1637	2394	2742	263	238	249	267	358	356	233	222	18
Ni	556	624	580	720	593	1034	1009	176	158	168	177	152	168	102	131	13
V	210	209	222	199	231	179	180	264	242	244	263	239	210	219	183	11
Zn	93	93	128	90	101	80	80	107	95	92	90	77	81	77	65	49
Rb	3	2	4	1	3	3	2					9			38	1
Ba	1	36	38	22	44	24	4	79	67	40	40	200	37	323	129	24
Sr	48	50	51	11	24	7	3	170	180	169	227	323	49	354	244	38
Nb	2.8	3.0	3.1	2.1	2.8	1.5	1.2	2.8	2.4	2.7	2.8	1.8	1.9	4.1	4.0	8.7
Hf	1.43	1.41	1.37	1.14	1.53	.91	.85	1.51	1.22	1.45	1.44	1.04	1.08	2.39	2.78	3.86
Zr	52	53	56	44	54	32	30	56	53	53	59	38	44	103	134	182
Y	12	12	13	11	13	9	10	18	17	17	18	13	13	17	14	22
Th	.25	.28	.21	.22	.24	.14	.10	.20	.20	.21	.24	.13	.22	1.08	1.20	3.93
La	3.32	2.80	2.62	1.84	2.29	1.08	1.04	2.77	2.55	2.80	2.82	1.74	1.92	10.73	12.47	18.70
Ce	8.56	7.94	7.69	5.85	6.85	3.43	3.10	7.47	6.99	7.63	7.44	5.00	5.38	26.21	27.77	41.69
Pr	1.25	1.20	1.20	.97	1.12	.56	.51	1.17	1.09	1.20	1.14	.79	.78	3.42	3.49	5.15
Nd	6.19	6.32	6.43	5.01	5.60	2.87	2.84	5.90	5.43	6.37	6.03	3.95	4.26	14.54	14.08	19.85
Sm	1.95	2.02	2.05	1.67	1.97	1.07	1.11	2.03	1.88	1.98	1.84	1.45	1.34	3.42	2.83	4.14
Eu	.64	.76	.67	.60	.64	.40	.37	.76	.64	.70	.80	.46	.46	1.07	.85	.62
Gd	2.37	2.52	2.45	2.05	2.48	1.49	1.56	2.68	2.61	2.78	2.62	2.01	1.72	3.22	2.85	4.18
Tb	.37	.41	.40	.34	.39	.27	.27	.47	.44	.45	.46	.34	.32	.51	.41	.61
Dy	2.48	2.50	2.56	2.21	2.73	1.84	1.89	3.28	2.82	3.20	3.11	2.36	2.24	3.66	2.49	3.97
Ho	.47	.50	.50	.42	.51	.37	.41	.73	.69	.71	.70	.51	.47	.67	.53	.79
Er	1.36	1.37	1.39	1.20	1.43	1.02	1.08	2.09	2.00	2.11	2.11	1.58	1.38	2.00	1.43	2.34
Tm	.20	.22	.20	.17	.20	.16	.17	.30	.32	.30	.30	.21	.20	.31	.22	.36
Yb	1.11	1.25	1.36	1.20	1.39	1.10	1.09	2.12	1.93	1.98	2.17	1.55	1.43	1.82	1.35	2.42
Lu	.20	.20	.21	.17	.19	.17	.17	.33	.28	.32	.32	.23	.23	.29	.20	.37

Mg# = 100 × (Mg/Mg + Fe_{tot}); SRG = Stoughton-Roquemaure Group; HMG = Hunter Mine Group; Transition Zone = Transition zone of the Hunter Mine Group; RAB = Rifted arc basalt (dike); AD = andesitic dike; Rhyolite = lava flows. Samples J-26 and J-28 described in Dostal and Mueller (1996).

processes, and constrain the depositional environment.

Transition Zone of the Hunter Mine Group. The aphanitic, microporphyritic, and locally porphyritic mafic lava flows, dikes, and sills have basaltic compositions (table 1; series WP). The mafic flows exhibit characteristic vertical and lateral volcanic facies variations (figure 3) that are common to modern arc-backarcs or mid-ocean ridges and are well-documented in Archean supracrustal sequences (Dimroth et al. 1978; Hargreaves and Ayres 1979; Wells et al. 1979). Very few flows, dikes, or sills are amygdaloidal. Flows are 3–20 m thick and have a massive columnar-jointed section grading vertically and laterally into pillowed flows or pillow breccia (figure 3). Pillows ranging from 20 to 150 cm in diameter display 0.5–2 cm thick chilled margins and internal polygonal jointing. In situ brecciation around pillows is common, but extensive pillow breccia units were not observed. Columnar joints within flows, ranging from 10 to 30 cm in diameter, are perpendicular to the cooling front. Some flows pinch out laterally with a 30° angle of repose (figure 3). Massive and columnar-jointed, mafic dikes represent the youngest phase in the felsic dike swarm (Dostal and Mueller 1996). Quench textures (e.g., ''swallow-tail'' plagioclase microlites) and spherulites characterize the border zones of pillows and massive flows.

Komatiite Units of the Stoughton-Roquemaure Group. Massive columnar-jointed and pillowed flow facies (figure 4*A*) constitute the komatiitic basalts and komatiites of the SRG. Flow breccias were rarely observed. Columnar-jointed units are 2–10 m thick and have sharp lower and upper contacts indicating a single flow unit. Joint columns are 10–40 cm in diameter, and column width is uniform throughout the flow. Millimeter to centimeter-scale pyroxene spinifex textures and non-oriented plumose pyroxene and plagioclase blades were transected by columnar joint growth. Ultramafic pillows and pillow tubes are 10-50 m thick (figure 4*A*) and up to several meters wide in transverse section (figure 4*B*). Individual pillow tubes are traceable for up to 10 m. The ends of pillow tubes flatten into a broad pancake shape up to 3 m wide and only 10–30 cm thick (figure 4*C,D*). Some tubes display longitudinal corrugations at the margins (figure 4*B*) and may possibly be a low viscosity counterpart to corrugation-B as described by Yamagishi (1985).

Flow surface features such as smooth half-moon ridges on branching (figure 5*A*) or individual pillow tubes indicate flow direction on the convex side for the most part. Central, longitudinal spreading cracks (figure 4*C* and 5*B*) facilitate subsequent pillow tube budding (figure 5*B*) that results from pulsating flow in the tubes. Symmetric and asymmetric transverse spreading cracks in the terminal pancake-shaped pillow are formed by decelerating flow velocity (figure 4*D*). Irregular to polygonal surface cracks (figure 5*C,D*) with local in situ hyaloclastite represent thermal contraction features that, in three dimensional exposures, locally transect the interior of the pillow. As flow decelerates and viscosity starts to affect flow morphology, tube-like pillowed flows start to show significant surface features. The typically smooth and flat-lying flow forms are a function of the high temperature and low viscosity of komatiitic magma. In the lower komatiite unit (figure 2), massive flows are generally higher in MgO (table 1; Roq-95-12) than the downslope pillowed flows (table 1; Roq-95-7). Lateral flow fractionation is inferred. Similarly, Barnes (1985) argued that fractionation in komatiite flows occurred because of olivine removal by spinifex growth and crystal settling. The morphological volcanic facies, dense character of komatiite lava, and absence of brecciation and amygdules possibly suggests extrusion under considerable water pressure, consistent with a deep-water setting. Sedimentary indicators, such as turbidite deposits and the absence of wave-induced structures, are consistent with this interpretation.

Petrography and Mineral Chemistry

Owing to the low degree of strain, the subgreenschist metamorphic grade has had little effect on primary volcanic textures. Relics of primary minerals, particularly clinopyroxene, are locally preserved. Calcic plagioclase is largely transformed to albite (An_{4-8}), and pyroxenes are generally altered to chlorite. Olivine is replaced entirely by serpentine and magnetite or by chlorite. The vitric groundmass is mostly altered to chlorite, albite, epidote, and Fe-Ti oxides, but quench textures are readily observed. Well-preserved chilled margins are composed of coalescing spherulites (figure 5*E*) representing an orb texture (Lofgren 1971) which grades, albeit abruptly, into quench microlites of hopper olivine and pyroxene (figure 5*F*). These quench textures are similar to those described by Dimroth et al. (1978) from the Archean mafic pillowed flows and by Lofgren (1980) from experimental studies. The komatiites and komatiitic basalts have classical spinifex textures of tabular, skeletal crystals of clinopyroxene (figure 5*G*). The massive parts of flows are characterized by open-fan spherulitic textures (figure 5*H*).

Clinopyroxenes in the tholeiitic basalts are au-

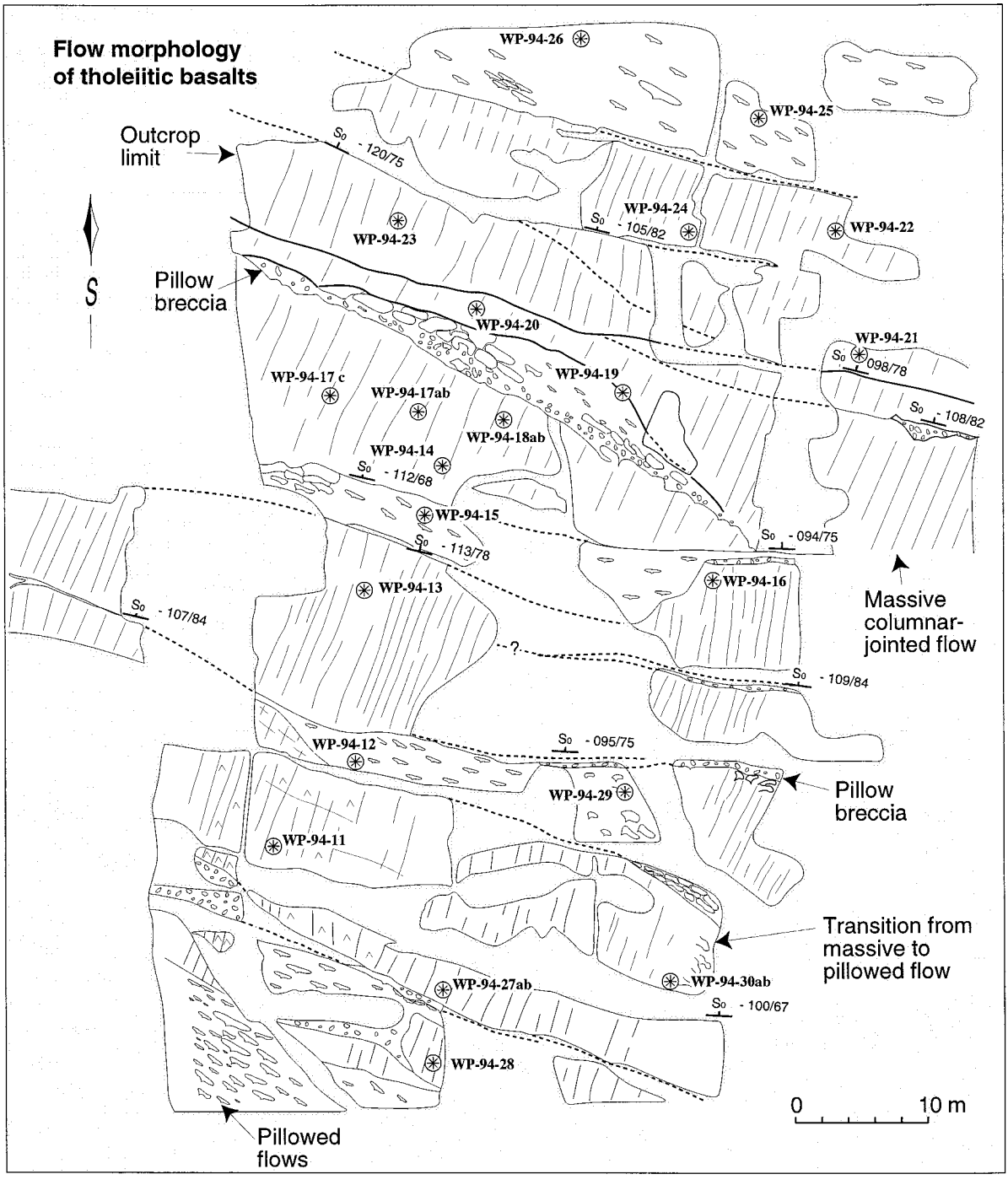

Figure 3. Transition zone of the HMG showing facies organization of tholeiitic basalts directly overlying the central part of the edifice. Note vertical and lateral facies changes in the studied section. The location is indicated in figure 2 (WP-94-2-30).

gites ($Wo_{30-40}En_{50-54}Fs_{10-16}$) according to the classification of Morimoto (1988). Phenocryst rims are slightly enriched in Fe ($Wo_{33}En_{48}Fs_{19}$). The komatiites and komatiitic basalts contain pyroxenes similar to those in other Archean sequences (Arndt et al. 1977; Fleet and MacRae 1975). In the komatiites, the composition of clinopyroxene ranges from predominantly diopside to augite ($Wo_{39-48}En_{38-49}Fs_{13-16}$), whereas the komatiitic basalts contain mainly augite ($Wo_{31-44}En_{39-54}Fs_{10-16}$) with a composition similar to those of the tholeiitic basalts. In general, the clinopyroxene of komatiites has lower

Si but higher Al and Ti than that of the tholeiific basalts. The high Al content in komatiite pyroxenes is due to either rapid growth of pyroxene and/or suppression of plagioclase crystallization (Donaldson 1982). According to the discrimination scheme of Leterrier et al. (1982), clinopyroxenes in the SRG have compositions characteristic of nonorogenic volcanic rocks.

Geochemistry

Analytical Techniques. Representative samples of lava flows from the transition zone (figure 3), the SRG, and the HMG were collected during mapping. Underlying felsic dikes and associated mafic and intermediate dikes and flows of the HMG were studied by Dostal and Mueller (1996) and are used for comparative purposes. Seventy-one samples of lava flows and related dikes have been analyzed for major and some trace (Rb, Sr, Ba, Zr, Nb, Y, Cr, Ni) elements using X-ray fluorescence at Saint Mary's University, Halifax. Twenty-seven samples were chosen for determination of a wider range of trace elements, including rare earth elements (REE), Th, Nb, and Hf using inductively coupled plasma mass spectrometry at Memorial University of Newfoundland. Results are given in table 1 (the complete data set is available upon request from *The Journal of Geology*). Precision and accuracy are discussed in Dostal et al. (1986, 1994). In general, the precision is better than ±2% for major elements and 2–10% for trace elements. Nine of the 27 samples were selected for Nd isotope analyses. Sm and Nd abundances and isotope ratios (table 2) were analyzed by isotope dilution mass spectrometry at Memorial University. A description of the analytical technique was given in Kerr et al. (1995). Mineral compositions were determined using a JEOL Superprobe 733 at Dalhousie University, Halifax, Nova Scotia.

Alteration. Sea-floor alteration and low-grade metamorphism was accompanied by selective chemical modifications as reflected by high LOI contents of the analyzed samples (table 1). On figures 7 to 9, whole rock analyses have been recalculated to 100% totals on an anhydrous basis. Low-temperature hydrothermal alteration of mafic-ultramafic rocks affected elements prone to movement such as Rb, K, and Na (e.g., Barnes 1985; Arndt and Jenner 1986); thus consideration of petrogenesis is based mainly on trace elements thought to be relatively "immobile." These include high field strength elements (HFSE), REE and transition elements (Winchester and Floyd 1977). Compositional similarities between the studied rocks and recent volcanic suites and comparisons with rather pristine komatiitic rocks from the Belingwe greenstone belt (Nisbet et al. 1993) suggest that in most samples these trace elements and most major elements retained their original abundances.

Stoughton-Roquemaure and Hunter Mine (Transition Zone) Groups. Volcanic rocks of the SRG and the transition zone of the HMG can be chemically divided into two groups. The first group includes tholeiitic basalts, which occur in the transition zone and the SRG, while the second group is characterized by komatiitic rocks, which are only present in the SRG (figure 6). The basalts have SiO_2 and MgO (LOI-free) ranging from 48.5% to 53.5% and from 6.5% to 13%, respectively (figure 7), and the Mg# [$= 100 \times Mg/(Mg + Fe_{tot})$] ranging from 67 to 49. The basalts have tholeiitic variation trends. Both Ti and V show positive correlations with incompatible trace elements, including Zr and P. These variations preclude extensive fractionation of Fe-Ti oxides. On classification diagrams involving Al, Fe, Ti, and Mg, the basalts generally plot in the field of Mg-rich tholeiitic basalts (figure 6). The basalts have relatively high contents of TiO_2 and Ni (figure 7) compared to recent island arc tholeiites (IAT), and resemble MORB. Their chondrite-normalized REE patterns are slightly light REE (LREE)-depleted to flat, with $(La/Yb)_n$ ratios (n-chondrite normalized) from 0.65 to 1 and abundances of about 5 to 10 times chondrites (figure 8*C*). The basalts are slightly less depleted in LREE than average N-MORB (figure 8*D*).

The tholeiitic basalts can be subdivided into high-Mg basalts and MORB-like basalts according to their Mg# and MgO contents. High-Mg basalts have higher Mg# (67–58) and MgO (9–13%) contents but lower abundances of incompatible trace

Figure 4. Characteristics of komatiites in the SRG. (*A*) Columnar-jointed komatiite flow (CJ: sample Roq-95-12) in sharp contact with pillowed flows (P). Top indicated by arrows. Scale: field notebook 20 cm long. (*B*) Close-up of a pillow tube showing a smooth flow surface with polygonal thermal contraction features (Tc) and longitudinal corrugations at the tube margin (Lc). Large arrow shows flow direction. Scale: large arrow 8 cm in size. (*C*) Pancake-shaped komatiite pillow with longitudinal (LSR) and transverse spreading ridge (TSR). Flow direction shown by two arrows. Scale: field notebook 20 cm long. (*D*) Flat, pancake-shaped, terminal end of pillow tube with a well-defined transverse spreading crack (TSR). Flow direction shown by two arrows. Sample location of Roq-95-9 indicated (S). Scale: field notebook 20 cm long.

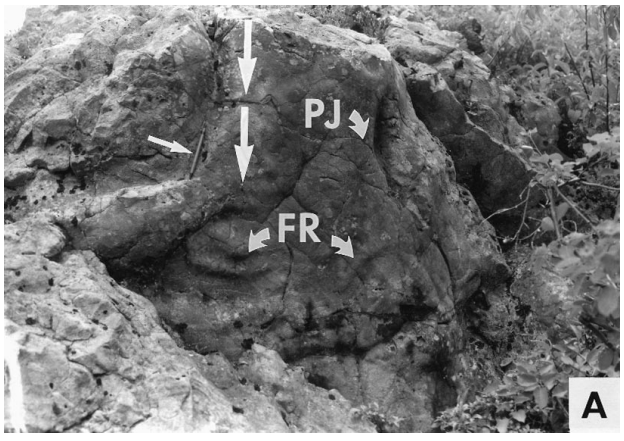

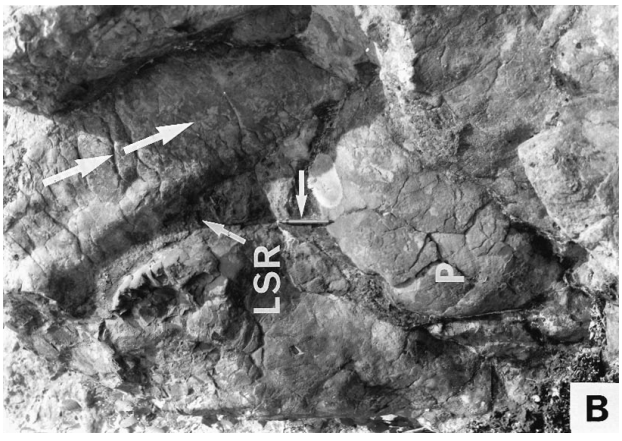

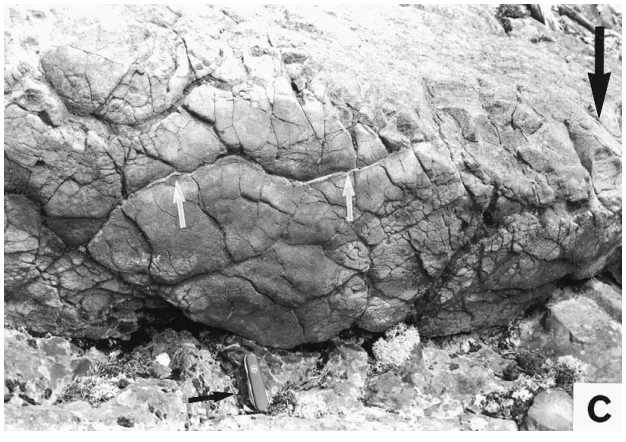

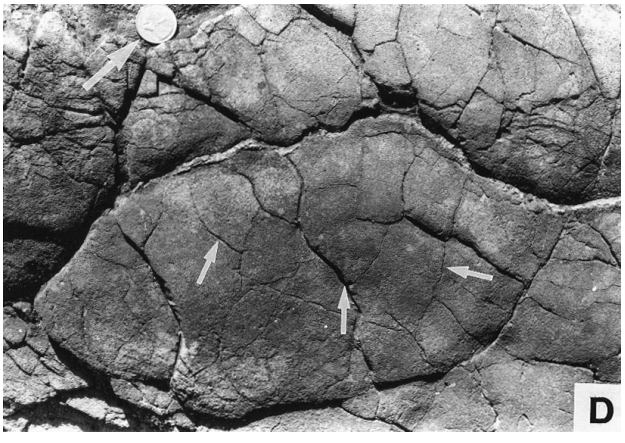

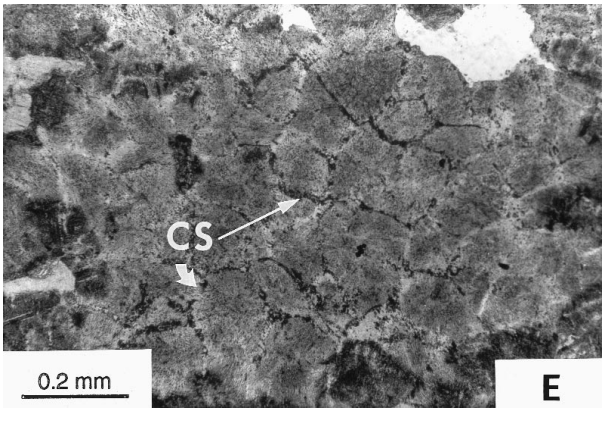

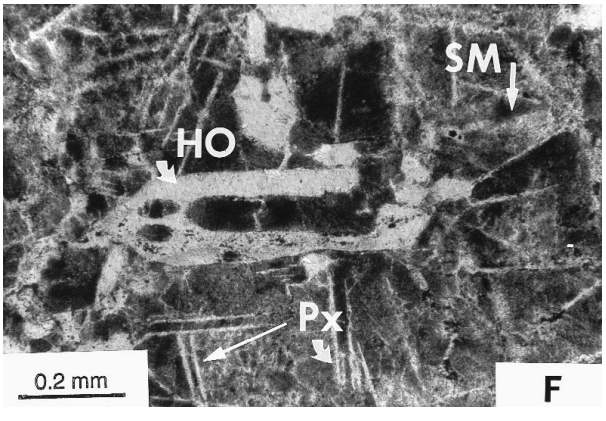

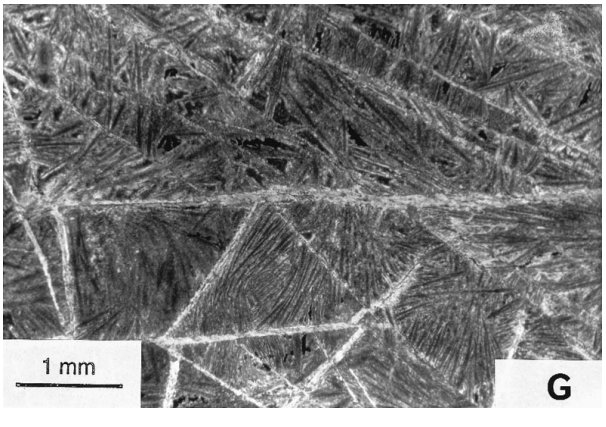

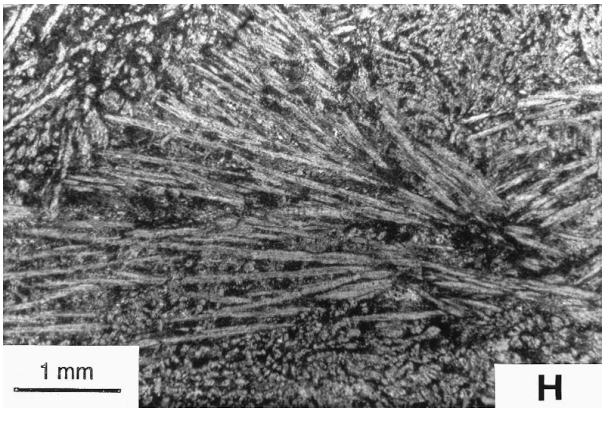

Table 2. Nd Isotopic Compositions of the SRG and HMG Rocks

Sample	Rock[a]	Sm (ppm)	Nd (ppm)	$^{147}Sm/^{144}Nd$	$^{143}Nd/^{144}Nd$[b]	ϵ_{Nd}[c]
HMG						
J-26	RAB	12.95	12.61	.1398	.511681 (9)	+1.3
Transition Zone						
WP-94-12	B	1.69	5.36	.1944	.512839 (8)	+4.7
WP-94-26	B	1.42	4.79	.1834	.512608 (11)	+4.1
J-22	B	1.40	4.17	.2002	.512831 (9)	+2.5
WP-94-27	HMB	1.17	3.85	.1872	.512888 (11)	+8.2
SRG						
Roq-95-7	KB	2.08	7.22	.1777	.51532 (11)	+4.6
Roq-95-12	KB	1.57	5.17	.1875	.512643 (9)	+3.3
Roq-95-15	K	1.13	3.83	.1817	.512658 (13)	+5.6
Roq-95-20	K	1.03	2.89	.2205	.513245 (17)	+3.5

[a] RAB = rifted arc basalt (dike); B = MORB-like tholeiitic basalt; HMB = high-Mg basalt; KB = komatiitic basalt; K = komatiite.
[b] Measured $^{143}Nd/^{144}Nd$ ratios are normalized to a $^{146}Nd/^{144}Nd$ of 0.7219. Errors for $^{143}Nd/^{144}Nd$ ratios are 2-sigma, given in parentheses. The La Jolla Standard, analyzed as part of every run, yielded average $^{143}Nd/^{144}Nd$ of 0.511856 ± 4 (2-sigma).
[c] ϵ_{Nd} were calculated at 2730 Ma (U-Pb zircon age of Mortensen, 1987) using present-day values for CHUR (chondritic uniform reservoir): $^{143}Nd/^{144}Nd_{CHUR} = 0.512638$ and $^{147}Sm/^{144}Sm_{CHUR} = 0.1967$.

elements (table 1) than the MORB-like basalts. The latter have Mg# ranging from 58 to 49 and MgO contents from 6.5% to 9% (table 1). Although both basalt groups have similar La/Yb and Th/Yb, they have different Cr/Ni and Ti/V, with high-Mg basalts having higher Cr/Ni (2.1–2.6 and 1.4–1.7, respectively) but lower Ti/V (15–18 and 19–23, respectively). The contrast between these two subgroups is in part due to fractional crystallization but also to a different source composition. The mantle-normalized trace element plots of the tholeiitic basalts (figure 9*C*) are not depleted in Nb, as would be expected from arc-related rocks; they are compositionally similar to T-MORB and oceanic plateau tholeiites (Storey et al. 1991). The initial ϵ_{Nd} values for the basalts (table 2) vary from +2.5 to + 8.2, suggesting derivation from a depleted mantle source and an absence of contamination by older continental crust during their evolution (DePaolo 1988).

The komatiites of the SRG include two distinct types: (1) komatiitic basalts (SiO_2 47–54%; Mg# 74–69) from the lower komatiitic unit, and (2) komatiites (SiO_2 44–47%; Mg# 77–78) that occur mainly in the upper komatiite unit (figure 2). Compared to tholeiitic basalts, both types of komatiitic flows usually have lower abundances of Fe, V, and incompatible trace elements, but higher MgO and transition elements. Komatiitic basalts have 14 to 20% MgO, $Al_2O_3 < 10\%$, $Al_2O_3/TiO_2 \sim 10$, $CaO/Al_2O_3 = 1–1.3$ and $(Gd/Yb)_n = 1.4–1.8$ (figure 10). Their REE have 5–10 times chondritic abundances and $(La/Yb)_n = 0.9–1.8$ (figure 8). HFSE concentrations are unfractionated relative to REE on primitive mantle concentration plots (figure 9). Like the komatiites, the patterns for komatiitic basalts do not exhibit a Nb depletion. The rocks resemble alumina-depleted komatiites that occur in 3.5 Ga suites but are rare in greenstone belts of 2.7 Ga age (Herzberg 1995).

The komatiites have MgO contents around 23% with $Al_2O_3/TiO_2 = 20$, $CaO/Al_2O_3 = 0.8$ and $(Gd/Yb)_n \sim 1–1.2$ (figure 10). In addition, they have slightly LREE depleted [$(La/Yb)_n \sim 0.5$] REE pat-

Figure 5. Surface features of komatiite pillow tubes and microscopic characteristics of komatiites in the SRG. (*A*) Branching of Archean komatiitic pillow tube with polygonal jointing (PJ) and half-moon flow ridges (FR). Flow direction shown by two arrows. Scale: pen 15 cm long (arrow). (*B*) Budding of a komatiitic pillow tube (P) from a central longitudinal spreading ridge (LSR). Sample location of Roq-95-10. Flow direction shown by two arrows. Scale: pen 15 cm long (arrow). (*C*) Summital part of pillow tube characterized by quenching causing fracturing of the surface and ingestion of water into the heart of the pillow tube (arrows). Scale: knife 9 cm long. (*D*) Close-up of thermal contraction features. Note polygonal jointing (arrows). Scale: coin 3 cm in diameter. (*E*) Microphotograph showing coalescing spherulites (CS) at a chilled pillow margin indicating an orb texture. (*F*) Microphotograph of quench textures with hopper olivine (HO), skeletal pyroxene (Px), and a spherulitic matrix (SM) between quench crystals. (*G*) Microphotograph of micro-pyroxene spinifex texture. (*H*) Microphotograph of open fan-spherulitic texture composed of skeletal pyroxene.

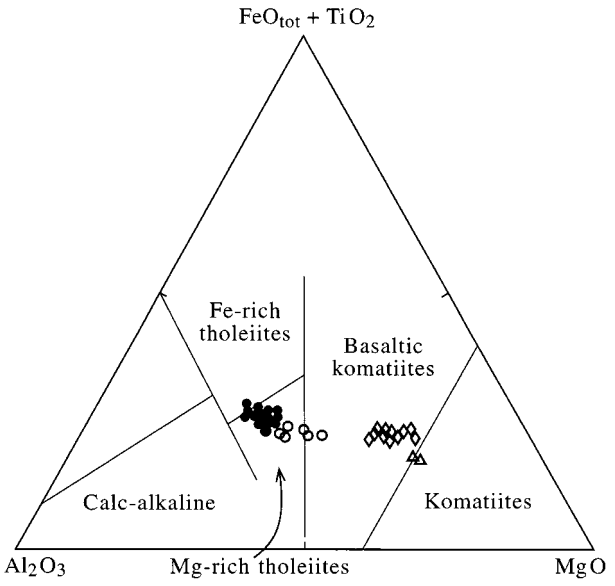

Figure 6. Classification of the rocks from HMG and SRG using a Jensen (1976) plot. Symbols: open triangles = komatiites; open diamonds = komatiitic basalts; open circles = high-Mg basalts; solid circles = MORB-like basalts. Several analyses not plotted because of overlap.

terns and 3–6 × chondritic abundances. Compositionally, komatiites have $(Gd/Yb)_n$ and Al_2O_3/TiO_2 close to those of chondrites (figure 10) and are similar to Munro-type, alumina-undepleted komatiites of the Abitibi belt that are the predominant type in 2.7 Ga greenstone belts (Herzberg 1995).

The initial ϵ_{Nd} values of the komatiites and komatiitic basalts are overlapping, ranging from +3 to +6 (table 2). These values also overlap the ϵ_{Nd} values of the associated MORB-like tholeiitic basalts. Some of these values are, however, slightly higher than those obtained on primary pyroxenes from komatiites of the Abitibi belt (Lahaye et al. 1995).

Hunter Mine Group. The rocks of the dike swarm and associated lava flows are mainly felsic (>65% SiO_2). Basaltic and andesitic rocks are present in only minor amounts (Dostal and Mueller 1996; table 1) and differ compositionally from the SRG and the HMG transition zone basalts. The HMG basaltic and andesitic dikes (e.g., sample J-26; table 1) and subordinate flows have chondrite-normalized REE profiles moderately enriched in LREE and $(La/Yb)_n$ ratios around 4 (figure 8). Their mantle-normalized incompatible trace element patterns (figure 9) have depleted Nb and enriched

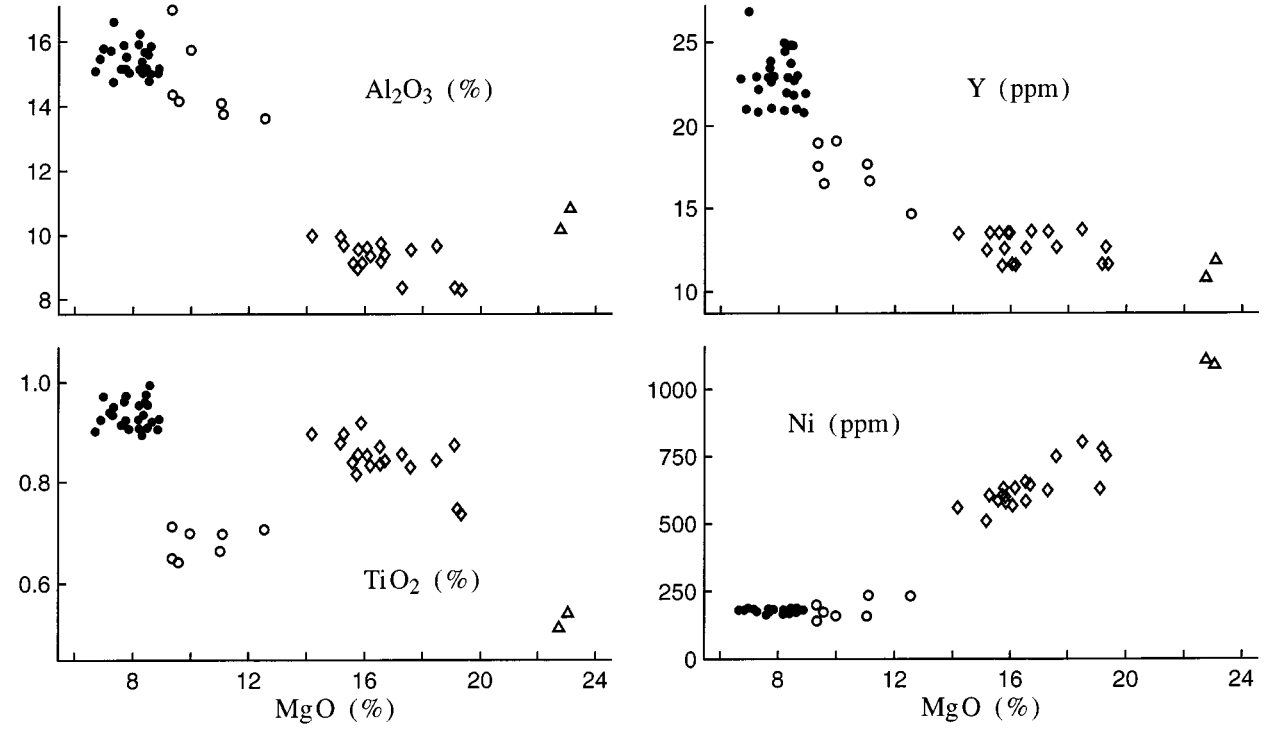

Figure 7. Al_2O_3 (%), TiO_2 (%), Y (ppm) and Ni (ppm) versus MgO (%) for the rocks of the transition zone and SRG group. Symbols: open triangles = komatiites; open diamonds = komatiitic basalts; open circles = high-Mg basalts; solid circles = MORB-like basalts.

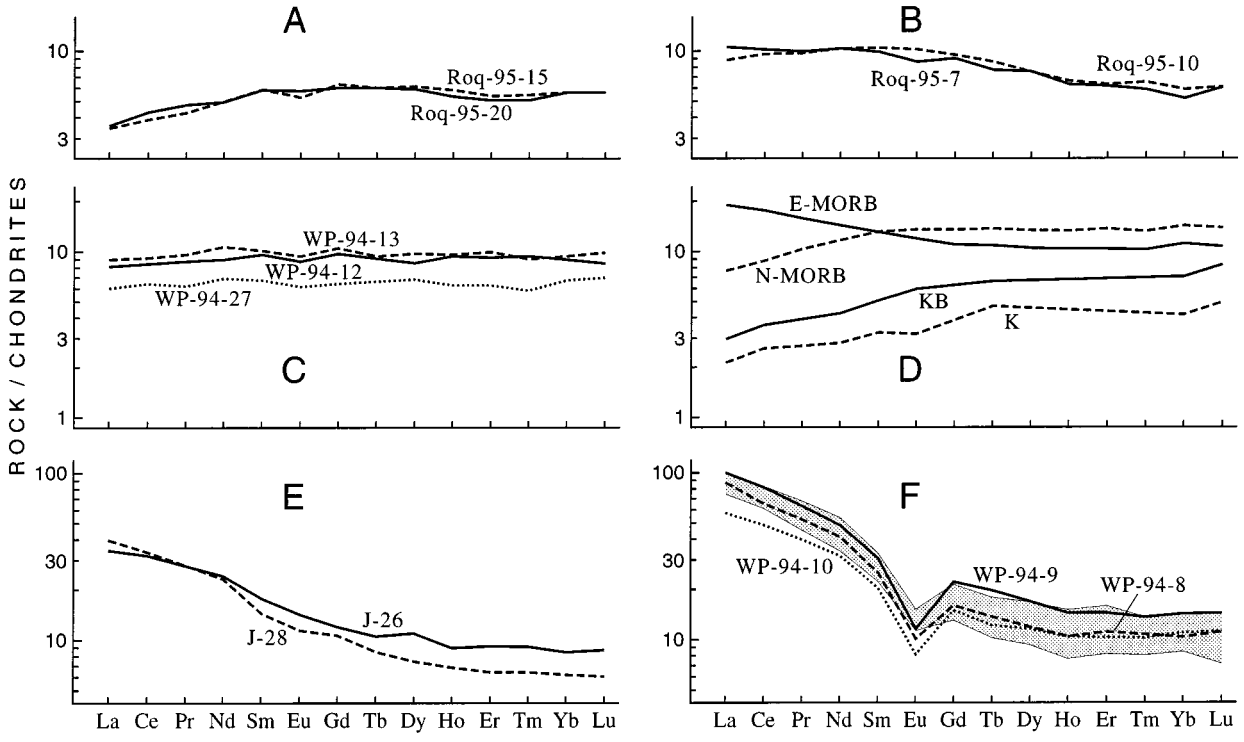

Figure 8. Rare-earth element abundances normalized to chondrites (after Sun 1982) for the rocks of HMG and SRG. (*A*) Al-undepleted komatiites of SRG. (*B*) Al-depleted komatiitic basalts of SRG. (*C*) high-Mg basalts (WP-94-27) and MORB-like basalts (WP-94-12, WP-94-13) of the transition zone of HMG. (*D*) N-MORB and E-MORB (after Sun and McDonough 1989) and average compositions of komatiites (K) and komatiitic basalts (KB) from Belleterre-Angliers belt (Barnes et al. 1993) shown for comparison. (*E*) rifted arc tholeiites of HMG. (*F*) HMG rhyolites (shaded field-range of the HMG felsic dikes; Dostal and Mueller 1996).

large-ion-lithophile elements (LILE) and REE. Compared to typical IAT, the basaltic rocks are enriched in Ti, Ni, and Cr (table 1; sample J-26) and resemble rocks formed in both modern and ancient island arc rift zones (e.g., Stern et al. 1990; Gamble et al. 1995).

Overall, the trace element compositions of the felsic dikes and lava flows are similar to calc-alkaline dacites and rhyolites elsewhere in the Abitibi belt (Ujike and Goodwin 1987; Dostal and Mueller 1992; Barrie et al. 1993). REE patterns are moderately enriched in LREE and have a small negative Eu anomaly (figure 8). Their $(La/Yb)_n$ ratios range from 5 to 8. Mantle-normalized incompatible element patterns have a moderate enrichment of Th and LREE relative to heavy REE (HREE) with a progressive increase toward Th (figure 9). The patterns are characterized by negative Nb and Ti anomalies and are comparable to modern subduction-related felsic rocks. The HMG mafic rocks range in ϵ_{Nd} from +1.0 to +2.5, and the felsic rocks range from +1.9 to +3.4 (Dostal and Mueller 1996). These values, particularly those of the felsic rocks, are close to the ϵ_{Nd} values of depleted mantle assumed to underlie the Abitibi belt at 2.7 Ga (+2.6 ± 0.8; Machado et al. 1986).

Petrogenesis

Stoughton-Roquemaure Group. The association of alumina-depleted and alumina-undepleted types is rare in greenstone belts. A similar joint occurrence in space and time has been documented in Newton Township west of Munro Township (Cattell and Arndt 1987) and could be of comparable origin. Because Al, Ti, and HREE are relatively immobile during alteration, differences between the two komatiite types in Al_2O_3/TiO_2 and Gd/Yb are inferred to be of magmatic origin.

Several processes that could account for the association of Al-depleted and Al-undepleted komatiitic rocks and the differences between them include (a) crustal contamination, (b) fractional crystallization, and (c) partial melting/source composition.

a) Crustal Contamination. Komatiitic magmas are thought to be prone to crustal contamination, in part, because of their high temperature and inferred turbulent flow (Huppert and Sparks 1985). El-

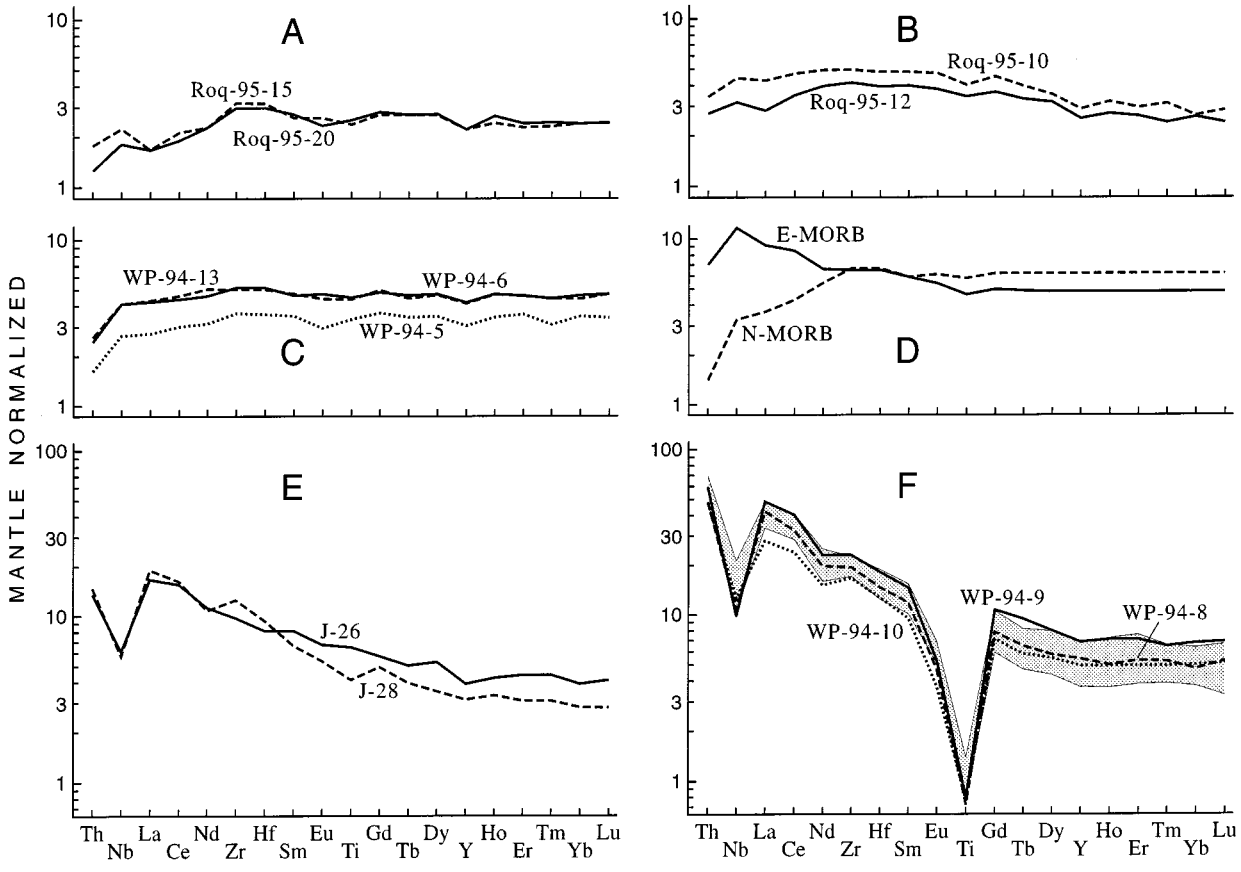

Figure 9. Mantle-normalized incompatible trace element patterns for the rocks of HMG and SRG. (*A*) Al-undepleted komatiites of SRG. (*B*) Al-depleted komatiitic basalts of the SRG. (*C*) high-Mg basalts (WP-94-5) and MORB-like basalts (WP-94-6, WP-94-13) of the transition zone of HMG. (*D*) N-MORB and E-MORB (after Sun and McDonough 1989) shown for comparison. (*E*) rifted arc tholeiites of HMG. (*F*) HMG rhyolites (shaded field = range of the HMG felsic dikes; Dostal and Mueller 1996). Normalizing values after Sun and McDonough (1989).

ement ratios diagnostic of crustal contamination show the largest difference between crust and a primitive mantle or komatiitic composition. Jochum et al. (1990) showed that element ratios such as Th/Nb, La/Nb, and Th/La are very sensitive measures of contamination. The values of these ratios in the SRG komatiites and komatiitic basalts are very low (~0.1; 1.0 and 0.10, respectively), unlike those affected significantly by crustal contamination (bulk continental crust 0.32, 1.45, and 0.22, respectively; Hofmann 1988). In addition, the ϵ_{Nd} values imply that the komatiitic rocks and tholeiitic basalts were not modified by interaction with older continental crust. Thus, the extent of contamination in SRG komatiites appears, at most, to be very small although they overlie the rhyolitic rocks of the HMG. The large contrast in Al_2O_3/TiO_2, CaO/Al_2O_3, and $(Gd/Yb)_n$ ratios (figure 10) between the two komatiitic types in conjunction with overlapping Th/Nb, La/Nb, and Th/La ratios and ϵ_{Nd} values is also inconsistent with crustal contamination being the cause of the differences between the two komatiite types.

b) Low-Pressure Fractional Crystallization. Crystallization of komatiitic magma at low pressure involves olivine, chromite, and pigeonite or augitic clinopyroxene (Kinzler and Grove 1985). Clinopyroxene crystallization is unlikely to have contributed to differences between the two komatiite types, because both types have comparable abundances of Ca. The separation of olivine and chromite, minerals with very low contents of incompatible trace elements, cannot significantly modify $(Gd/Yb)_n$ ratios, suggesting that the observed differences between the two types are not due to fractional crystallization.

c) Different Degrees of Partial Melting/Differences in Source Compositions. There is a growing consensus that differences between Al-depleted and Al-undepleted komatiites are related to the role of garnet in their source (e.g., Herzberg 1995). As discussed below, the available data for the SRG ko-

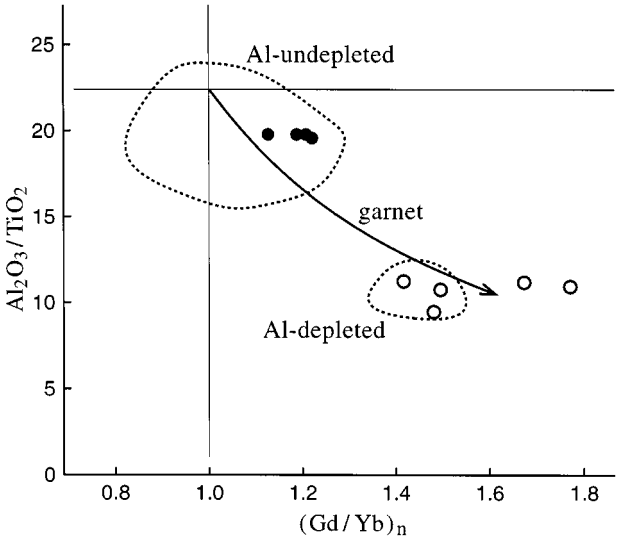

Figure 10. Variations of Al_2O_3/TiO_2 versus $(Gd/Yb)_n$ (n = chondrite-normalized) in SRG komatiitic rocks compared to the fields for Al-depleted and Al-undepleted komatiites of Lahaye et al. (1995) and a trend showing the effect of fractionation of garnet (after Lahaye et al. 1995). The arrow on the curve represents increasing garnet in the melting residue. Symbols: open circles = Al-depleted komatiitic basalts; solid circles = Al-undepleted komatiites. The lines correspond to chondritic values of the corresponding ratios.

matiitic lavas are compatible with this model. The low concentrations of incompatible trace elements and their ratios in both komatiite types are, in general, consistent with their derivation from a source slightly depleted in incompatible elements relative to a primitive mantle composition.

Origin of the Komatiites. Two models have frequently been advocated to explain the origin of komatiites: (1) Allegre (1982) suggested a subduction-related genesis. Subduction of an oceanic plate could lead to hydration of the overlying mantle wedge, which in turn would lower the mantle solidus temperature (e.g., Gallagher and Hawkesworth 1992); thus komatiites could be generated by a large degree of melting at relatively shallow depths. This mechanism can account for the widespread association of komatiites with subduction-related rocks frequently observed in Archean greenstone belts. However, the lack of Nb depletion as well as the non-orogenic composition of clinopyroxenes in the komatiitic rocks is not consistent with this hypothesis. The model does not readily explain the association of komatiites with MORB-like basalts as well as the association of the two komatiite types.

2) Campbell et al. (1989) argued that komatiites were formed by melting induced by mantle plumes. Komatiites are inferred to be derived from the hotter axial parts of the plume, whereas tholeiitic basalts are derived from the cooler plume head or material entrained by the upwelling plume. The composition of the SRG komatiites and associated komatiitic and tholeiitic basalts, including their mantle-normalized patterns and Nd isotopes, is consistent with such a model.

The spatial and temporal association of Al-depleted and Al-undepleted komatiitic lavas with distinct chemical compositions puts additional constraints on komatiite petrogenesis. Low Al_2O_3/TiO_2 and fractionated HREE that characterize Al-depleted komatiitic rocks are usually attributed to the presence of garnet in the residue after mantle melting (Ohtani et al. 1989; Gruau et al. 1990; Herzberg 1992, 1995). On the other hand, the Al-undepleted Munro-type komatiites, which have chondritic Al_2O_3/TiO_2 and flat HREE patterns, were probably formed by high degrees of melting, leaving only olivine ± orthopyroxene in the residue (Lahaye et al. 1995). Alternatively, the Al-undepleted komatiites could have been generated by melting of a garnet-free source, possibly at shallower depth. Figure 10 compares variations of critical major and trace element ratios in the SRG komatiitic rocks with other komatiites and gives a curve showing the effects of increasing garnet in the melting residue (after Lahaye et al. 1995). The plot shows that the composition of Al-depleted komatiitic basalts is consistent with garnet fractionation, whereas the Al-undepleted komatiites can be produced by melting leaving a garnet-free residue. It suggests that both types were derived from a common source by variable degrees of melting. Lower MgO contents of the Al-depleted komatiitic basalts suggest that these rocks were generated by a lower degree of melting than Al-undepleted komatiites, leaving garnet in the melting residue. A higher degree of melting required for Al-undepleted komatiites consumed all garnet, and the melting residue is garnet-free. Thus, it is possible that both komatiitic types were derived at approximately the same depth by different degrees of partial melting.

On the basis of experimental data, Herzberg (1995) concluded that two associated komatiitic types from Newton Township were derived from a common source. The Al-depleted types were inferred to be solidus melts formed at 5–7 GPa (depth of about 150–200 km) at the periphery of a plume, whereas the Al-undepleted komatiites were formed by a higher degree of melting in the plume axis. Such a plume is probably about 200°C hotter than ambient 2.7 Ga mantle (Herzberg 1995). This pressure estimate is consistent with the presence of py-

rope garnet rather than majorite in the source. Garnet changes from pyrope to majorite at pressures in excess of 14 GPa (~400 km) (Herzberg et al. 1990; Herzberg 1995).

Hunter Mine Group. The differences between the incompatible trace element signatures of the HMG and SRG basalts (figures 8 and 9) suggest different sources. The HMG basaltic and andesitic rocks (table 1; figure 9; samples J-26 and J-28) have subduction-related characteristics with a negative Nb anomaly and enrichments in the LILE and LREE, similar to backarc basin basalts or rift-related arc basalts (e.g., Stern et al. 1990; Gamble et al. 1995). They are interpreted to be formed by melting of a mantle source previously modified by subduction processes. In contrast, the overlying SRG basalts were derived from a MORB-type or plume type source and are not related to the rhyolites or the HMG basalts. Assuming that the HMG source was altered by subduction, this modification did not affect the isotope systematics, suggesting that no long-lived subduction component was added to the HMG source. Depleted mantle-like ϵ_{Nd} values for the felsic rocks imply that the rocks were either formed by fractionation of mafic melts or from melting of mantle-derived material with a short crustal residence time (Dostal and Mueller 1996). Dostal and Mueller (1996) proposed that rhyolitic rocks of the HMG were formed by partial melting of underplated basalts or gabbros at a middle or lower crustal depth with subsequent differentiation.

Geodynamic Setting

The large (600 × 200 km) NVZ of the Abitibi greenstone belt is considered to be a coherent tectonostratigraphic succession (figure 1) representing an ancient diffuse oceanic island arc (Chown et al. 1992; Mueller et al. 1996) that developed over a north-dipping Archean subduction zone (e.g., Calvert et al. 1995). The HMG, an integral part of the Abitibi arc (Mueller et al. 1996), represents a large subaqueous volcanic complex of volcanic cycle 1 that did not breach the ocean surface. The central dike complex is composed of rhyolitic-rhyodacitic dikes and minor rifted arc-related basaltic and andesitic dikes (Dostal and Mueller 1996). Formation of such an extensive rhyolitic dike system necessitates extension (Dostal and Mueller 1996). Arc splitting is characterized by abundant dike emplacement (Carey and Sigurdsson 1984). The geochemical signature of the HMG rhyolites and related mafic rocks, highlighted by Nb and Ti anomalies, supports a rifted arc setting and is consistent with the interpretation of the Abitibi greenstone belt as a complex island arc system (Mueller et al. 1989, 1996). Extension must have continued over a prolonged period of time because mafic dikes, which used the same conduits as the felsic dikes, were intruded after the main felsic constructional phase terminated. In contrast to central volcanic construction, the mafic-ultramafic units of the SRG reflect extensive effusive ocean floor volcanism. Volcanism of this nature is generally fissure-fed.

The rise of a mantle plume beneath and through the arc best explains mafic-ultramafic flooding of the volcanic arc complex. Basaltic magmas with geochemical characteristics of a rifted arc were probably generated by shallow melting of a mantle wedge above a subduction zone. The physical volcanology and geochemical signature of the HMG and SRG, and tectonic constraints suggest that rifting was initiated and enhanced by the plume. The plume may have also induced melting of a crustal source during the genesis of the rhyolitic rocks of the HMG. The komatiites are interpreted to represent the center of a mantle-derived plume with the maximum temperature and maximum degree of melting. The Al-depleted komatiitic basalts were probably formed at the same depth as the Al-undepleted komatiites but at the periphery of a plume. In this scenario, the tholeiitic basalts were generated in the cooler plume head. The flat HREE patterns of all tholeiitic basalts suggest melting at a shallow depth relative to the komatiites.

The stratigraphic succession in the SRG supports this interpretation. The tholeiitic basalts, both MORB-like and high Mg basalts, located at the base of the lower komatiite unit compare favourably to the initial cool part of the plume. As the plume evolves, deeper parts of the mantle are tapped as indicated by the komatiitic basalts and komatiites.

The stratigraphy reveals cyclicity between komatiite and basalt units possibly suggesting a pulsating plume that can be best explained by extrusion of magma from the cool part of the plume with subsequent replenishment from deeper levels. Because plumes are considered extensive features (hundreds of kilometers in diameter), the association of MORB-like basalts, high Mg basalts, Al-depleted komatiitic basalts, and Al-undepleted komatiites of the SRG is best explained as a lateral extremity of a plume that had periodic access (cause of cyclicity) to the deeper mantle. Komatiites associated with a subaqueous rifted arc setting, as suggested from this study, may be quite common. The Munro Township komatiites (Pyke et al. 1973), which are of comparable age and occur along strike, may be part of the same large-scale event.

Barrie et al. (1993) noted that komatiites may be intercalated with abundant felsic material. The depositional model of Barnes et al. (1993) for the Belleterre-Angliers belt, in which the plume-related magma traverses pre-existing arc crust, coincides with the interpretation proposed in this study. The association of rhyolites interstratified upward with MORB-like basalts and ultramafic rocks may thus be more widespread in Archean greenstone belts than hitherto observed.

Conclusions

The volcanic rocks of the HMG and SRG of the Archean Abitibi greenstone belt show the effects of a mantle plume rising below and through an arc. The HMG rocks, representing a submergent arc complex, feature an extensive felsic-dominated dike swarm (Dostal and Mueller 1996) that exhibits the geochemical signature of a rifted arc. The rising plume facilitated melting of the mafic oceanic crust to form the HMG felsic rocks. Contemporaneous melting of the mantle wedge can account for the generation of the rifted arc-related basalts in the HMG. The rise of the basaltic and komatiitic melts followed pre-existing zones of weakness, as exemplified by the extensive HMG-feeder dike complex.

The SRG, characterized by the association of komatiites, komatiitic basalts, and MORB-like tholeiitic basalts, is inferred to be the result of melting of an Archean mantle plume. An unusual association of Al-depleted and Al-undepleted komatiites reflects the different role of garnet in their genesis. Garnet was probably a residual phase during the partial melting of the Al-depleted komatiitic basalts. In contrast, the Al-undepleted komatiites were generated either at a shallower depth by melting of a garnet-free mantle source, or alternatively, were higher-degree melts, leaving only a harzburgitic residue. The latter model is favored. The Al-undepleted komatiites represent the central hot part of the plume, whereas the Al-depleted basaltic komatiites were formed closer to the periphery of the plume. The tholeiitic basalts (MORB-like and high Mg basalts) were generated from the cooler head of the rising plume at a significantly shallower depth. The occurrence of the komatiites in an arc setting may be more common in Archean supracrustal successions than previously recognized.

ACKNOWLEDGMENTS

This research was supported by NSERC operating grants to both authors and Lithoprobe funding to WUM (Lithoprobe contribution 862). The manuscript benefitted from the reviews of J. V. Owen as well as the incisive comments of editor A. T. Anderson, and Journal reviewers L. Ayres and R. Stern.

REFERENCES CITED

Allégre, C. J., 1982, Genesis of Archean komatiites in a wet ultramafic subducted plate, *in* Arndt, N. T., and Nisbet, E. G., eds., Komatiites: London, George Allen and Unwin, p. 495–500.

Anhaeusser, C. R., 1971, Cyclic volcanicity and sedimentation in the evolutionary development of Archaean greenstone belts of Shield areas: Geol. Soc. Australia Spec. Pub., v. 3, p. 57–70.

Arndt, N. T., 1994, Archean komatiites, *in* Condie, K. C., ed., Archean Crustal Evolution: Amsterdam, Elsevier, p. 11–44.

———, and Jenner, G. A., 1986, Crustally contaminated komatiites and basalts from Kambalda, Western Australia: Chem. Geol., v. 56, p. 229–255.

———; Naldrett, A. J.; and Pyke, D. R., 1977, Komatiitic and iron-rich tholeiitic lavas of Munro Township, northeast Ontario: Jour. Petrol., v. 18, p. 319–369.

———, and Nisbet, E. G., 1982, What is a komatiite? *in* Arndt, N.T., and Nisbet, E. G., eds., Komatiites: London, George Allen and Unwin, p. 19–27.

Barnes, S. J., 1985, The petrography and geochemistry of komatiite flows from the Abitibi greenstone belt and a model for their formation: Lithos, v. 18, p. 241–270.

———; Couture, J. F.; Sawyer, E. W.; and Bouchaib, C., 1993, Nickel-copper occurrences in the Belleterre-Angliers belt of the Pontiac Subprovince and the use of Cu-Pd ratios in interpreting platinum group element distributions: Econ. Geology, v. 88, p. 1402–1418.

Barrie, C. T.; Ludden, J. N.; and Green, T. H., 1993, Geochemistry of volcanic rocks associated with Cu-Zn and Ni-Cu deposits in the Abitibi Subprovince: Econ. Geol., v. 88, p. 1341–1358.

Bickle, M. J., and Nisbet, E. G., 1993, The geology of the Belingwe greenstone belt, Zimbabwe: Geol. Soc. Zimbabwe Spec. Pub. 2, 238 p.

———; ———; and Martin, A., 1994, Archean greenstone belts are not oceanic crust: Jour. Geology, v. 102, p. 121–138.

Calvert, A.; Sawyer, E. W.; Davis, W. J.; and Ludden, J. N., 1995, Seismic images of a mantle suture in the Superior Province: Evidence for Archean subduction: Nature, v. 375, p. 670–674.

Campbell, I. H.; Griffiths, R. W.; and Hill, R. I., 1989, Melting in an Archean mantle plume: Heads it's basalts, tails it's komatiites: Nature, v. 339, p. 697–699.

Carey, S., and Sigurdsson, H., 1984, A model of volcanogenic sedimentation in marginal basins, *in* Kokelaar, B. P., and Howells, M. F., eds., Marginal basin geology: Geol. Soc. London Spec. Pub. 16, p. 37–58.

Cattell, A., and Arndt, N. T., 1987, Low-and high-alumina komatiites from a Late Archean sequence, Newton Township, Ontario: Contrib. Mineral. Petrol., v. 97, p. 218–227.

Chown, E. H.; Daigneault, R.; Mueller, W.; and Mortensen, J., 1992, Tectonic evolution of the Northern Volcanic Zone, Abitibi belt, Quebec: Can. Jour. Earth Sci., v. 29, p. 2211–2225.

Corfu, F.; Krogh, T. E.; Kwok, Y. Y.; and Jensen, L. S., 1989, U-Pb zircon geochronology in the southwestern Abitibi greenstone belt, Superior Province: Can. Jour. Earth Sci., v. 26, p. 1747–1763.

DePaolo, D. J., 1988, Neodymium Isotope Geochemistry: Heidelberg, Springer-Verlag, 154 p.

de Wit, M. J.; Hart, R. A.; and Hart, R. J., 1987, The Jamestown ophiolite complex, Barberton Mountain belt: A section through 3.5 Ga oceanic crust: Jour. Afr. Earth Sci., v. 6, p. 681–730.

Dimroth, E.; Cousineau, P.; Leduc, M.; and Sanschagrin, Y., 1978, Structure and organization of Archean subaqueous basalt flows, Rouyn-Noranda area, Quebec, Canada: Can. Jour. Earth Sci., v. 15, p. 902–918.

Donaldson, C. H., 1982, Spinifex-textured komatiites: A review of textures, compositions, and layering, *in* Arndt, N. T., and Nisbet, E. G., eds., Komatiites: London, George Allen and Unwin, p. 213–244.

Dostal, J.; Baragar, W. R. A.; and Dupuy, C., 1986, Petrogenesis of the Natkusiak continental basalts, Victoria Island, NWT: Can. Jour. Earth Sci., v. 23, p. 622–632.

———; Dupuy, C.; and Caby, R., 1994, Geochemistry of the Neoproterozoic Tilemsi belt of Iforas (Mali, Sahara): A crustal section of an oceanic island arc: Precamb. Res., v. 65, p. 55–69.

———, and Mueller, W., 1992, Archean shoshonites from the Abitibi greenstone belt, Chibougamau (Quebec, Canada): Geochemistry and tectonic setting: Jour. Volcanol. Geother. Res. v. 53, p. 145–165.

———, and ———, 1996, An Archean oceanic felsic dike swarm in a nascent arc: The Hunter Mine Group, Abitibi greenstone belt, Canada: Jour. Volcanol. Geother. Res., v. 72, p. 37–57.

Dupre, B.; Chauvel, C.; and Arndt, N. T., 1984, Pb and Nd isotopic study of two komatiite flows from Alexo, Ontario: Geochim. Cosmochim. Acta, v. 48, p. 1965–1972.

Eakins, P. R., 1972, Roquemaure Township: Quebec Dept. Nat. Res. Geol. Rept. 150, 69 p.

Fleet, M. E., and MacRae, N. D., 1975, A spinifex rock from Munro Township, Ontario: Can. Jour. Earth Sci., v. 12, p. 928–939.

Gallagher, K., and Hawkesworth, C., 1992, Dehydration melting and generation of continental flood basalts: Nature, v. 358, p. 57–59.

Gamble, J. A.; Wright, I. C.; Woodhead, J. D.; and McCulloch, T. M., 1995, Arc and back-arc geochemistry in the southern Kermadec arc-Ngatoro basin and offshore Taupo volcanic zone, SW Pacific, *in* Smellie, J. L., ed., Volcanism associated with extension at consuming plate margins: Geol. Soc. London, Spec. Pub. 81, p. 193–212.

Goutier, J., 1993, Porcupine-Destor 5: Quebec Dept. Nat. Res., Rapport d'activit 93 (DV-93-02), 60 p.

Gruau, G.; Chauvel, C.; Arndt, N. T.; and Cornichet, J., 1990, Aluminum depletion in komatiites and garnet fractionation in the early Archean mantle: Hafnium isotopic constraints: Geochim. Cosmochim. Acta, v. 54, p. 3095–3101.

Hargreaves, R., and Ayres, L. D., 1979, Morphology of Archean metabasalt flows, Utik Lake, Manitoba: Can. Jour. Earth Sci., v. 16, p. 1452–1466.

Herzberg, C., 1992, Depth and degree of melting of komatiites: Jour. Geophys. Res., v. 97, p. 4521–4540.

———, 1995, Generation of plume magmas through time: An experimental perspective: Chem. Geolog., v. 126, p. 1–16.

———; Gasparik, T.; and Sawamoto, H., 1990, Origin of mantle peridotite: Constraints from melting experiments to 16.5 GPa: Jour. Geophys. Res., v. 95, p. 15,779–15,803.

Hofmann, A. W., 1988, Chemical differentiation of the earth: The relationship between mantle, continental crust, and oceanic crust: Earth Planet. Sci. Lett., v. 90, p. 297–314.

Huppert, H. E., and Sparks, R. S. J., 1985, Cooling and contamination of mafic and ultramafic magmas during ascent through continental crust: Earth Planet. Sci. Lett., v. 74, p. 371–386.

Jensen, L. S., 1976, A new cation plot for classifying subalkalic volcanic rocks: Ontario Division of Mines MP 66, 22 p.

Jochum, K. P.; Arndt, N. T.; and Hofmann, A. W., 1990, Nb-Th-La in komatiites and basalts: Constraints on komatiite petrogenesis and mantle evolution: Earth Planet. Sci. Lett., v. 107, p. 272–289.

Kerr, A.; Jenner, G. A.; and Fryer, B. J., 1995, Sm-Nd isotopic geochemistry of Precambrian to Paleozoic granitoid suites and the deep-crustal structure of the southeast margin of the Newfoundland Appalachians: Can. Jour. Earth Sci., v. 32, p. 224–245.

Kinzler, R. J., and Grove, T. L., 1985, Crystallization and differentiation of Archean komatiite lavas from northeast Ontario: Phase equilibrium and kinetic studies: Am. Mineral., v. 70, p. 40–51.

Lahaye, Y.; Arndt, N. T.; Byerly, G.; Chauvel, C.; Fourcade, S.; and Gruau, G., 1995, The influence of alteration on the trace-element and Nd isotopic compositions of komatiites: Chem. Geology, v. 126, p. 43–64.

Leterrier, J.; Maury, R.C.; Thonon, P.; Girard, D.; and Marchal, M., 1982, Clinopyroxene composition as a method of identification of the magmatic affinities of paleo-volcanic series: Earth Planet. Sci. Lett., v. 59, p. 139–154.

Lofgren, G. E., 1971, Experimentally produced devitrification textures in natural rhyolite glass: Geol. Soc. America Bull., v. 82, p. 111–124.

———, 1980, Experimental studies on the dynamic crystallization of silicate melts, *in* Hargraves, R. B., ed., Physics of Magmatic Processes: Princeton, NJ, Princeton University Press, p. 487–551.

Machado, N.; Brooks, C.; and Hart, S. R., 1986, Determi-

nation of initial $^{87}Sr/^{86}Sr$ and $^{143}Nd/^{144}Nd$ in primary minerals from mafic and ultramafic rocks: experimental procedure and implications for isotopic characteristics of the Archean mantle under the Abitibi greenstone belt, Canada: Geochim. Cosmochim. Acta, v. 50, p. 2335–2348.

Morimoto, N., 1988, Nomenclature of pyroxenes: Mineral. Mag., v. 52, p. 535–550.

Mortensen, J. K., 1987, Preliminary U-Pb zircon ages for volcanic and plutonic rocks of the Noranda-Lac Abitibi area, Abitibi Subprovince, Quebec: Geol. Survey Canada Paper 87-1A, p. 581–590.

———, 1993*a*, U-Pb geochronology of the eastern Abitibi Subprovince: Part 1: Chibougamau-Matagami-Joutel: Can. Jour. Earth Sci., v. 30, p. 11–28.

———, 1993*b*, U-Pb geochronology of the eastern Abitibi Subprovince. Part 2: Noranda-Kirkland Lake area: Can. Jour. Earth Sci., v. 30, p. 29–41.

Mueller, W.; Chown, E. H.; Sharma, K. N. M.; Tait, L.; and Rocheleau, M., 1989, Paleogeographic and paleotectonic evolution of a basement-controlled Archean Supracrustal sequence, Chibougamau, Quebec: Jour. Geology, v. 97, p. 399–420.

———; Daigneault, R.; Mortensen, J. K.; and Chown, E. H., 1996, Archean terrane docking: Upper crust collision tectonics, Abitibi greenstone belt, Quebec, Canada: Tectonophysics, v. 265, p. 127–150.

———, and Donaldson, J. A., 1992*a*, Development of sedimentary basins in the Archean Abitibi belt, Canada: An overview: Can. Jour. Earth Sci., v. 29, p. 2249–2265.

———, and ———, 1992*b*, A felsic feeder dike swarm formed under the sea: The Archean Hunter Mine Group, south-central Abitibi belt, Quebec, Canada: Bull. Volcanol., v. 54, p. 117–134.

Nisbet, E. G.; Martin, A.; Bickle, M. J.; and Orpen, J. L., 1993, The Ngezu Group: Komatiites, basalts, and stromatolites on continental crust, *in* Bickle, M. J., and Nisbet, E. G., eds., The Belingwe Greenstone Belt, Zimbabwe: A study of Archean continental crust: Geol. Soc. Zimbabwe Spec. Pub. 2, p. 121–165.

Ohtani, E.; Kawabe, I.; Moriyama, J.; and Nagata, Y., 1989, Partitioning of elements between majorite garnet and melt and implications for petrogenesis of komatiite: Contrib. Mineral. Petrol., v. 103, p. 263–269.

Pyke, D. R.; Naldrett, A. J.; and Eckstrand, O. R., 1973, Archean ultramafic flows in Munro Township, Ontario: Geol. Soc. America Bull., v. 84, p. 955–978.

Stern, R. J.; Lin, P. N.; Morris, J. D.; Jackson, M. C.; Fryer, P.; Bloomer, S. H.; and Ito, E., 1990, Enriched back-arc basin basalts from the northern Mariana Trough: Implications for the magmatic evolution of back-arc basins: Earth Planet. Sci. Lett., v. 100, p. 210–225.

Storey, M.; Mahoney, J. J.; Kroenke, L. W.; and Saunders, A. D., 1991, Are oceanic plateaus sites of komatiite formation?: Geology, v. 19, p. 376–379.

Sun, S. S., 1982, Chemical composition and origin of the earth's primitive mantle: Geochim. Cosmochim. Acta, v. 46, p. 179–192.

———, and McDonough, W. F., 1989, Chemical and isotopic systematics of oceanic basalts: Implications for mantle composition and processes, *in* Saunders, A. D., and Norry, M. J., eds., Magmatism in the Ocean Basins: Geol. Soc. London Spec. Pub. 42, p. 313–345.

Takahashi, E., 1990, Speculations on the Archean mantle: Missing link between komatiite and depleted garnet peridotite: Jour. Geophys. Res., v. 95, p. 15,941–15,954.

Thurston, P. C., and Chivers, K. M., 1990, Secular variation in greenstone sequence development emphasizing Superior Province, Canada: Precamb. Res., v. 46, p. 21–58.

Ujike, O., and Goodwin, A. M., 1987, Geochemistry and origin of Archean felsic metavolcanic rocks, central Noranda area, Quebec, Canada: Can. Jour. Earth Sci., v. 24, p. 2551–2567.

Winchester, J. A., and Floyd, P. A., 1977, Geochemical discrimination of different magma series and their differentiation products using immobile elements: Chem. Geol., v. 20, p. 325–343.

Wells, G.; Bryan, W. B.; and Pearce, T. H., 1979, Comparative morphology of ancient and modern pillow lavas: Jour. Geology, v. 87, p. 427–440.

Yamagishi, H., 1985, Growth of pillow lobes-evidence from pillow lavas of Hokkaido, Japan, and North Island, New Zealand: Geology, v. 13, p. 499–502.